

CFD Technology for Rotorcraft Gearbox Windage Aerodynamics Simulation

Matthew J. Hill, Robert F. Kunz, Ralph W. Noack,
Lyle N. Long, Philip J. Morris and Robert F. Handschuh

*(Presented at the American Helicopter Society 64th Annual Forum, Montreal, Canada, April 29–May 1, 2008.
Copyright 2008 by the American Helicopter Society International, Inc. All rights reserved.)*

Management Summary

A computational fluid dynamics (CFD) method is adapted, validated and applied to spinning gear systems with emphasis on predicting windage losses. Several spur gears and a disc are studied. The CFD simulations return good agreement with measured windage power loss. Turbulence modeling choices, the relative importance of viscous and pressure torques with gear speed and the physics of the complex 3-D unsteady flow field in the vicinity of the gear teeth are studied.

Introduction

Gearbox windage refers to the power losses associated with rotational deceleration torques exerted on spinning gears by aerodynamic forces (pressure and viscous) within the air-oil atmosphere in a gearbox. Windage losses are a source of significant heating and fuel consumption in rotorcraft and other systems. Rotorcraft systems require the gearing components to be lightweight and heavily loaded. The components are also required to operate at high rotational speeds where windage losses become significant with respect to other gearbox losses (rolling, sliding and lubrication) Windage losses are relevant to aircraft design for several reasons:

1) They can consume several percent of the transmitted power. This has significant implications for onboard oil cooling requirements and lube system capacity, thereby compromising range and standby military readiness for rotorcraft and carrier-based aircraft.

2) Rotorcraft platform survivability under transmission *oilout* conditions is exacerbated by windage losses, which are manifested as added dissipative flow heating to these already critically thermally stressed systems.

Despite this significant relevance, design efforts aimed at reducing gearbox windage losses have generally fallen into the trial and error category. Nevertheless, it has been shown by Winfree (Ref. 1) and others that modest geometric modi-

fications to control the air flow path, such as shrouding and baffle configurations, can significantly reduce both windage losses and lubricating oil consumption (80% and 40% reductions observed respectively [Ref. 1]). However, these hardware-specific approaches are empirical, expensive and time consuming, and to be relevant, they need to be performed late in the design cycle.

A host of experimental studies have appeared in the literature (Refs. 1–8). These studies employ either closed-loop systems (Refs. 2–6) or treat isolated gears (Refs. 1, 7 and 8) where windage (and other) losses are determined by measuring spin-down velocities once the gear and shaft assembly is disconnected from the drive torque. Figure 1 shows a diagram of the high-speed helical gear train test facility at the NASA Glenn Research Center. It is a closed-loop system that has been set up to study the thermal behavior of aerospace-quality gear components under various speeds, loads and lubricant flow rates (Ref. 5). These studies parameterize gear geometry elements, rotational speed, enclosure geometry and lubrication system characteristics (flow rate, jet location, lubricant rheology), using dimensional analysis to develop correlations for the power losses. These correlations, although useful in the design process, are inherently limited by the large number of system variables and the attendant limited range of their applicability. Of particular concern here is the paucity of data/correlations available for high-speed gears of interest. Indeed, compressibility effects are mostly not even considered in the literature, although high-speed gears can have tip Mach numbers reaching 0.75.

Unfortunately, the physics of these systems are so complex that to date there have been no attempts made to employ many modern elements of 3-D computational fluid dynamics (CFD) in analyzing gearbox windage. Recent 2-D studies (Ref. 9) were performed using the commercial CFD solver FLUENT, where a side correlation factor was used to account for 3-D effects (although these authors state that work is under way to extend their simulations to 3-D) (Ref. 10). Specifically, the fluid mechanics involve complex, separated air flow, disperse multiphase flow (oil droplets),

continuous multiphase films (lubricating oil on gears), moving boundaries in contact and all modes of heat transfer. Accordingly, for a CFD tool to resolve all of the relevant physics of this problem, it must:

- support moving meshes (either adaptive/deforming or overset) necessary to resolve the gears in relative motion and contact at the gear face;
- contain non-equilibrium multiphase flow capability (separate continuity and momentum equations for each phase; slip between phases) to accommodate the disperse mist/droplet and continuous film flows;
- support suitable turbulence modeling to accommodate the complex high-speed, separated flow within the gearbox and to accurately represent the cascade of energy through turbulence scales into viscous heating;
- possess suitable preconditioned time-stepping algorithms to efficiently accommodate Mach numbers ranging from near-zero through high-subsonic;
- support conduction, convection and (for near-failure conditions) radiation modeling;
- be parallelized to run efficiently on modern high-performance computing (HPC) systems.

Theoretical Formulation Governing Equations

Governing equations. The conservation of mass, momentum and energy can be written in integral conservation law form for a compressible flow through a moving mesh as:

$$\frac{\partial}{\partial t} \int_V \rho dV + \int_S \rho (\underline{V} - \underline{W}) \cdot d\underline{S} = 0 \quad (1)$$

$$\frac{\partial}{\partial t} \int_V \rho \underline{V} dV + \int_S \rho \underline{V} (\underline{V} - \underline{W}) \cdot d\underline{S} = - \int_S p d\underline{S} + \int_S \underline{\tau} \cdot d\underline{S} \quad (2)$$

$$\frac{\partial}{\partial t} \int_V \rho E dV + \int_S \rho H (\underline{V} - \underline{W}) \cdot d\underline{S} = \int_S (\underline{\tau} \cdot \underline{V}) \cdot d\underline{S} + W_f + q_H \quad (3)$$

In equations 1–3, \underline{V} is the velocity vector, and \underline{W} is the velocity of the surface element $d\underline{S}$, both in the absolute frame of reference. In the present work, all verification and validation flows studied are either incompressible, or they have maximum local absolute Mach numbers of less than 0.35. Accordingly, for all simulations presented in this paper, an incompressible assumption is invoked and the energy equation is not solved (except for the thermal Couette flow simulation where it is solved subject to a constant density constraint).

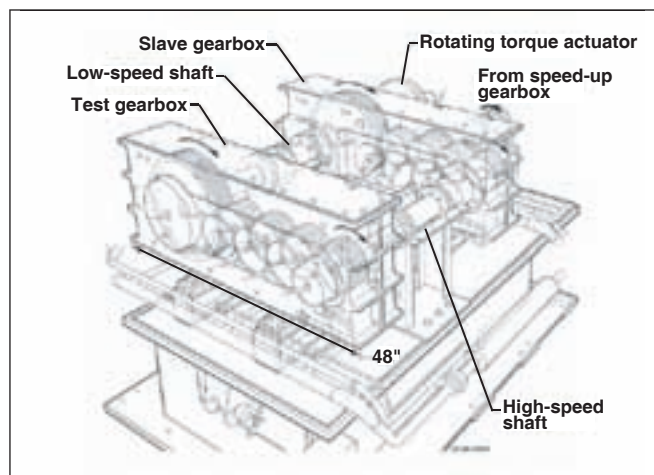


Figure 1—NASA High-Speed Helical Gear Train Facility (Ref. 5).

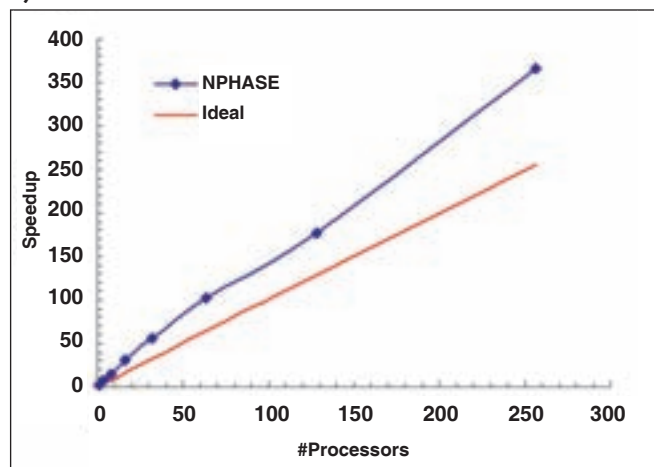


Figure 2—Parallel efficiency of NPHASE-PSU on Columbia system for a 1.1×10^5 cell spinning cylinder case.

A high-Reynolds number $k-\epsilon$ turbulence model and a sublayer resolved hybrid $k-\epsilon/k-\omega$ turbulence model, due to Menter (Ref. 11), are used in the studies that follow. No explicit transition model was employed as justified, for now, by the small contribution of near-axis viscous torques on windage loss.

CFD numerics and code. The CFD code used in this work, NPHASE-PSU (Ref. 12), is a parallel face-based, cell-centered, arbitrary-element unstructured multiphase flow solver which has been instrumented with overset mesh capability. The baseline algorithm follows established, segregated pressure-based methodology. A co-located variable arrangement is used and a lagged coefficient linearization is applied (Ref. 13). Diagonal dominance-preserving, finite-volume spatial discretization schemes are used for the scalar transport equations. Continuity is introduced through a pressure correction equation, based on the SIMPLE-C algorithm (Ref. 14). In constructing cell face fluxes, a momentum interpolation scheme (Ref. 15) is employed, which introduces damping in the continuity equation. Grid motion/deformation terms are implemented in a Geometric-Conservation-Law (GCL) preserving fashion (Ref. 16). A dual-time formulation is employed where at each physical time-step, between five

continued

and 20 pseudo time-steps of the SIMPLE-C algorithm are applied. Specifically, at each pseudo time-step, the discrete momentum equations are solved approximately (using a simple point iterative scheme), followed by a more exact solution of the pressure correction equation (using the *PETSC* (Ref. 17) *parallel LU pre-conditioning + GMRES utilities*).

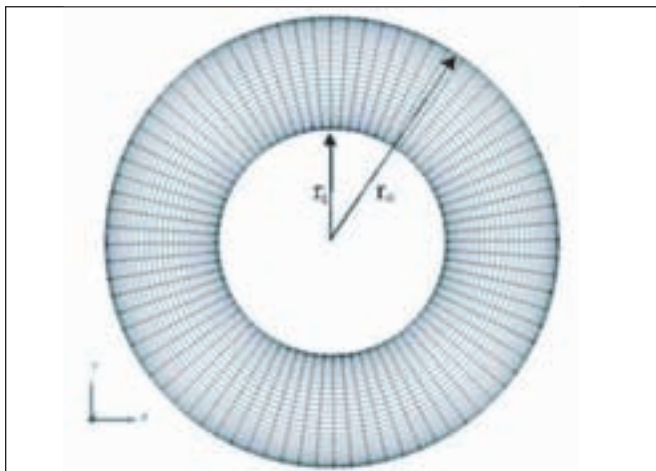


Figure 3—Computational domain for the rotating Couette flowcase.

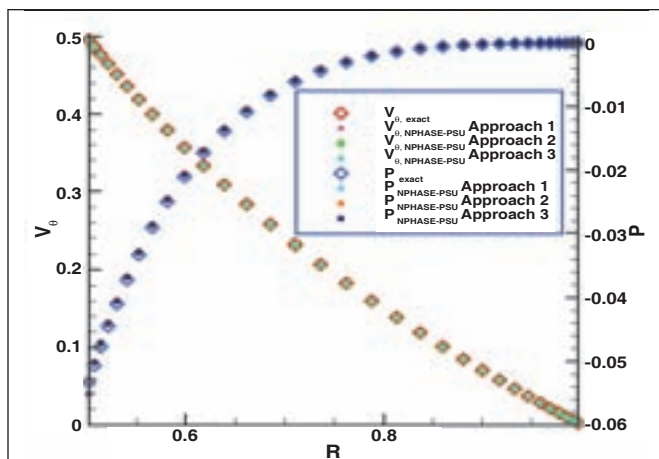


Figure 4—Comparison of NPHASE-PSU and analytical solutions for the rotating Couette flow case.

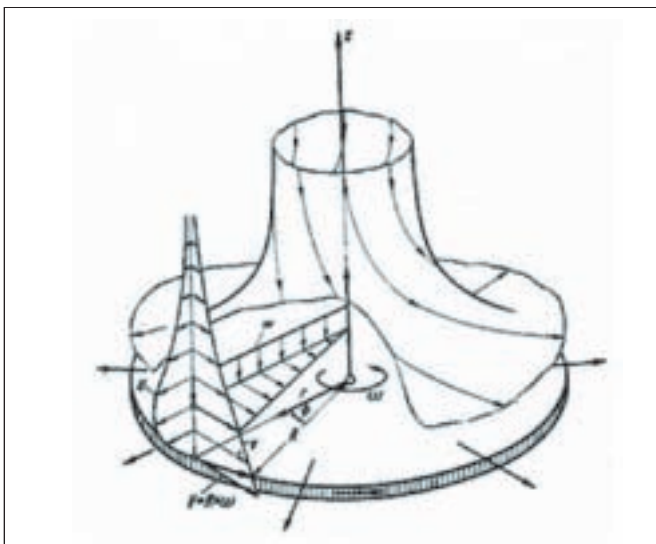


Figure 5—Sketch of the flow field in the vicinity of an infinite span rotating disc.

Turbulence scalar and energy equations are then solved in succession. Parallelization is implemented in a standard fashion by invoking domain decomposition based on *METIS* (Ref. 18) in the front end, and MPI-based message passing in the CFD code. All of the large-scale simulations presented in this paper were executed on the Columbia supercomputer at NASA Ames Research Center. The code scales very well on this system, as illustrated in Figure 2.

DiRTlib and SUGGAR. The overset grid approach (Ref. 19) utilizes a composite grid consisting of a set of overlapping component grids to discretize the domain. No point-to-point or face-to-face matching is required between component grids. The solution on the component grids is linked by identifying appropriate intergrid boundary points (IGBPs) where the solution is given by a specified boundary value obtained by interpolation from another overlapping donor component grid. The overset domain connectivity information (DCI), which consists of the identification of the inter-grid boundary points and corresponding interpolation sources, is obtained by an overset grid assembly step. The current effort utilizes two overset software libraries to add the overset capability to *NPHASE-PSU*.

DiRTlib (Ref. 20), which stands for *Donor Interpolation Receptor Transaction library*, is a solver-neutral library that encapsulates the functionality required by the solver to utilize the overset domain connectivity information. It is independent of the solver grid storage and topology, dependent variables, etc., and can be used with any solver.

The current overset grid assembly process is performed using the *SUGGAR* code (Ref. 21), which stands for *Structured, Unstructured, Generalized overset Grid Assembler*. *SUGGAR* is a general overset grid assembly code with the capability to create the domain connectivity information at node and/or element centers for most current grid topologies, including any combination of structured Cartesian and curvilinear, unstructured tetrahedral and mixed element, general polyhedral and octree-based Cartesian grids. For static grid assemblies with no motion between component grids, the grid assembly is a pre-processing step. The case of solution and time-dependent motion requires the solver to communicate the new body and grid positions to the grid assembly process, wait for it to complete, and then load the new DCI. For the case of prescribed motion, such as used in the present study, the DCI is a-priori-computed and saved in a file for each time step in the simulation, and the solver simply loads the file appropriate for each time step.

The donor interpolations produced by *SUGGAR* are a set of linear weights that multiply the values at the donor members. For a cell-centered flow solver, such as *NPHASE-PSU*, the interpolation stencil will use as members the cell in the donor grid that was found to contain an IGBP and the neighboring cells that share a face with the donor cell. The interpolation weights are computed using an un-weighted, least-square procedure.

Results

Verification studies. In the context of the overset meshing strategy employed for gearbox windage simulations, the meshes will be in motion relative to one another. As indicated above, the approach taken here is to solve the flow in the absolute frame of reference for the entire computational domain, i.e., on all meshes—those that are rotating and those that are stationary. In order to verify that *NPHASE-PSU* correctly handles these gear-relevant rotating mesh systems, two verification studies were performed—rotating Couette flow, and flow near an infinite rotating disc—both of which have available analytical solutions.

Rotating Couette flow. Figure 3 is an illustration of the 33 x 81 (radial x azimuthal) computational domain for the incompressible rotating Couette flow case. The r_{inner} and r_{outer} boundaries are walls. In this case, inner = 0.5 and outer = 1.0. The outer cylinder is held stationary and a rotation rate of $\omega = 1\text{ s}^{-1}$ is specified for the inner cylinder. The Reynolds number independent analytical solutions for the tangential velocity and pressure are:

$$V_{\theta} = Cr \left(1 - \frac{1}{r^2} \right) \quad (4)$$

$$p = \rho \left(\frac{C^2 r^2}{2} - 2C^2 \ln(r) - \frac{C^2}{2r^2} \right) \quad (5)$$

$$C = -\frac{\omega}{3} \quad (6)$$

Figure 4 shows a comparison of the analytical solution with three *NPHASE-PSU* runs, designated Approaches 1, 2 and 3. Approach 1 solves the absolute velocities in the absolute frame on a stationary grid (adapting inner cylinder boundary conditions accordingly). Approach 2 solves for the relative velocities in the relative frame on a stationary grid (i.e., frame-of-reference rotating with angular velocity, ω , adapting the momentum equation source terms and outer-cylinder boundary conditions accordingly).

Approach 3 solves for absolute velocities in the absolute frame using a time-accurate analysis on a rotating mesh. Approach 3 is the most relevant for gear analysis. Figure 4 illustrates that the code returns the analytical solution for all three simulation approaches to within the accuracy of the second-order accurate discretization numerics and grid used.

Flow near an infinite rotating disc. The second verification case is a classic 3-D exact solution to the incompressible Navier-Stokes (N-S) equations. An infinite radial span disc rotates with an angular velocity, ω . This induces tangential flow in the direction of rotation, radial outflow and an axial flow towards the center of the disc. In this case, the N-S equations reduce to a system of non-linear ODEs, which can essentially be exactly solved numerically. Figure 5 is a notional sketch of the flow field from Schlichting (Ref. 22).

Figure 6 shows the 232,662-element unstructured mesh employed for the analysis. The extent of the computational domain was selected to be $r_{max} = 1.0$, $z_{max} = 1.0$. For a choice of $\omega = 1.0$ and $\mu = 1.0 \times 10^{-2}$, this domain provided that the

solution sampled within the region $r \leq 0.2$, $z \leq 0.4$ compares very closely with the exact solution despite the necessarily finite extent of the domain.

NPHASE-PSU was applied using two approaches. Approach 1 solves the absolute velocities in the absolute frame on a stationary grid (adapting disc boundary conditions accordingly). Approach 2 solves for absolute velocities in the absolute frame using a time-accurate analysis on a rotating mesh. Figure 7 illustrates that the code returns the exact solution for both simulations to within the accuracy of the second-order accurate discretization numerics and grid used.

Couette flow with wall heating. The third validation performed sought to verify the viscous dissipation term implementation in *NPHASE-PSU*. The relevance of viscous dissipation physics to gear windage is significant, as discussed above. The analytical solution for the temperature distribution in a laminar linear Couette flow was chosen. Figure 8 shows a diagram of the configuration. The product of the Prandtl number ($Pr \equiv \mu C_p / k$) and the Eckert number ($Ec \equiv U_i^2 / C_p (T_1 - T_0)$), $PrEc$, is a measure of the role of viscous dissipation in a flow. The nearly exact comparisons between CFD result and the analytical solution, shown in Figure 9, across a range of $PrEc$, illustrates that the viscous dissipation terms in *NPHASE-PSU* are implemented correctly.

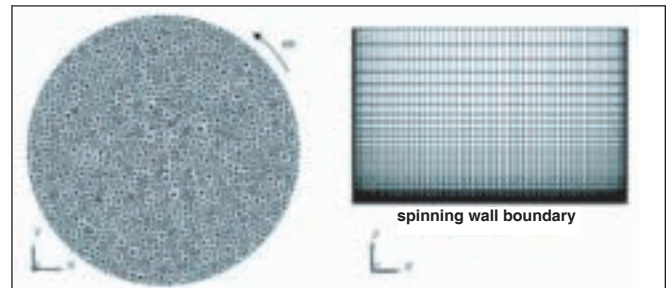


Figure 6—232662 element unstructured mesh employed for the infinite spanning rotating disc.

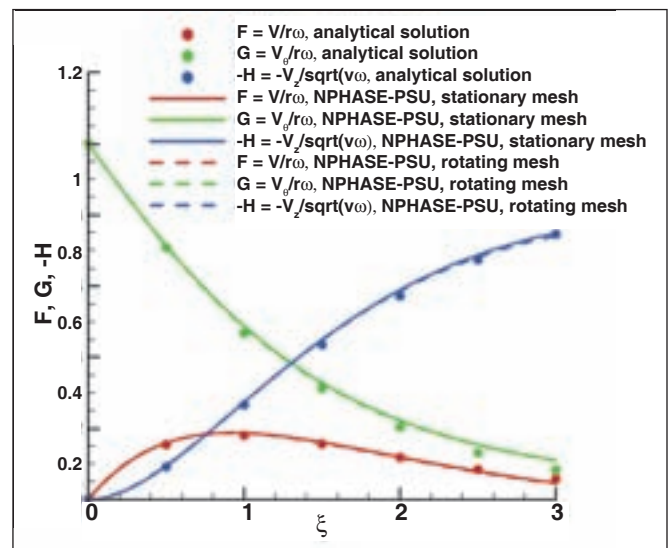


Figure 7—Comparison of *NPHASE-PSU* and exact solutions for the infinite span rotating disc.

Validation studies. The experimental data of Diab, et al. (Ref. 8) was used to validate *NPHASE-PSU* for the case of un-shrouded, isolated, rotating spur gears. Diab, et al. tested four different spur gears and a disc in free air on a spin-down test rig. The gears varied in diameter, width and tooth count. The properties of the gears and disc are provided in Table

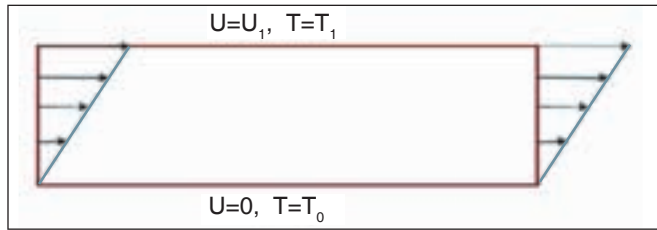


Figure 8—Illustration of the linear heated Couette flow case.

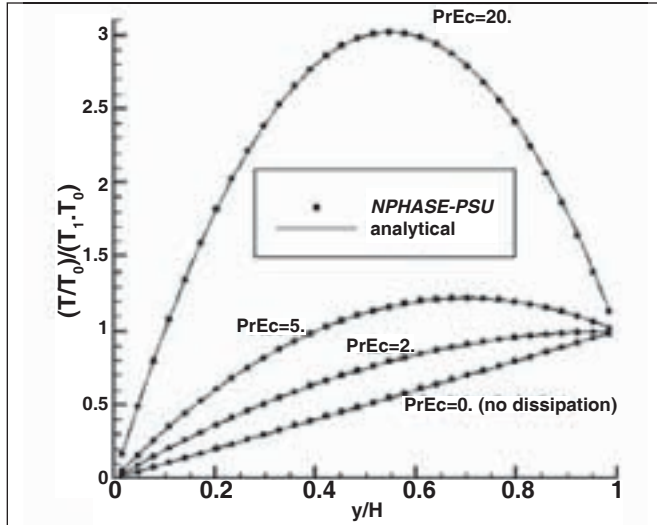


Figure 9—Comparison of *NPHASE-PSU* and exact solutions for the linear heated Couette flow case.

	Pitch Diameter(mm)	Tooth Width (mm)	Module (mm)
Gear 1	288	30	4
Gear 2	144	30	4
Gear 3	144	60	4
Gear 4	144	60	6
Disk	300	30	

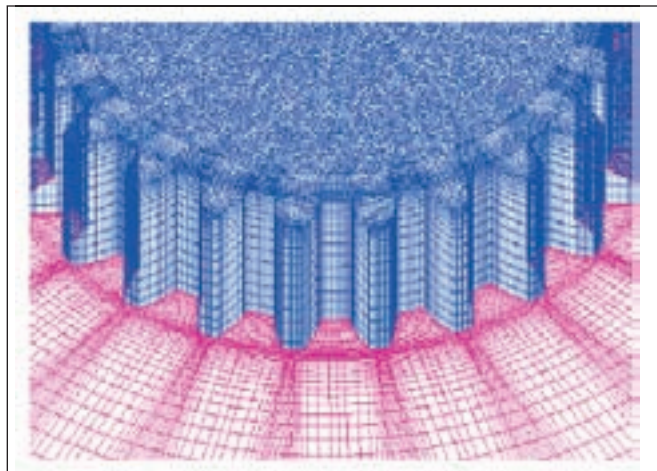


Figure 10—Grid topology of Gear 4.

1. Diab, et al, did not study the effects of gear enclosure or lubrication. A sequence of prescribed constant rotation rate simulations was used to replicate the experiment.

Single grid simulations. Grids were generated for all four spur gears and the disc. For the gear studies where the high-Reynolds number $k-\epsilon$ turbulence model was used, near-

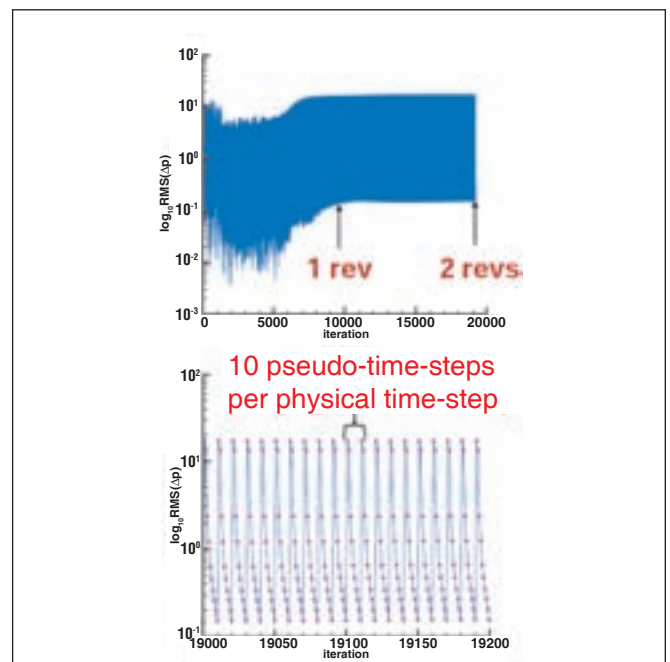


Figure 11—Example convergence history for Diab Gear 4.

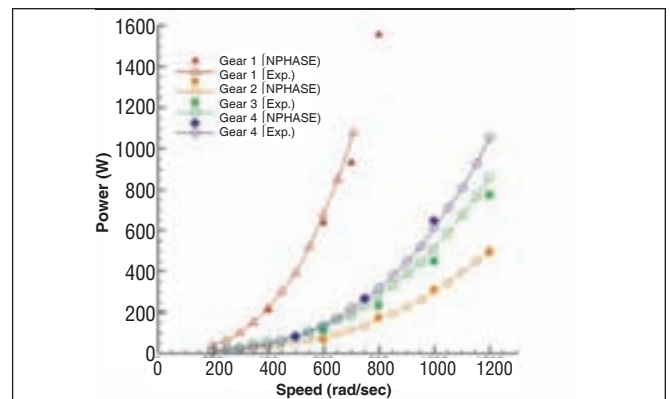


Figure 12—Comparisons between the experimental results and the *NPHASE-PSU* analysis.

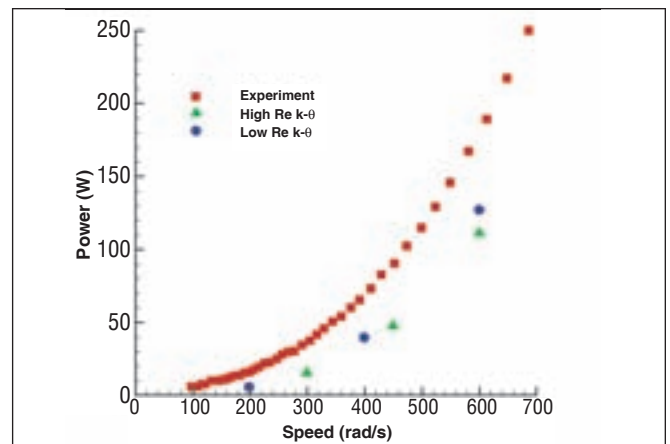


Figure 13—Effect of turbulence model selection on viscous work prediction.

wall grid spacing was defined to accommodate wall-functions (e.g., $y^+ \approx 70$ for gear 1, $\omega = 1000\text{s}^{-1}$). The single plane of symmetry in the problem was exploited to reduce total cell count by a factor of 2. Grid cell counts for the different cases varied between 2×10^6 (Gear 4) and 8×10^6 (Gear 1). Grid generation was further simplified by employing a hybrid mesh topology, as illustrated in Figure 10. Specifically, for the regions above the surface of the gear teeth to the outer boundary, structured hexahedral cells were used. For the region above the gear face surface, unstructured prism cells were employed. The meshes were generated using the commercial grid generation software package *Gridgen* (Ref. 23). The computational domain of the isolated gear grids was extended to approximately five times the gear radius from the gear surface in all directions. This distance was adequate for defining a symmetry boundary condition since the flow is nearly stagnant there.

An azimuthal step size of 1/40th of one tooth passage duration (the time it takes one tooth to rotate to the position of the tooth adjacent to it) was used in all CFD calculations. This corresponds to 2,880 time-steps-per-gear revolution for Gear 1, 1,440 time steps for Gears 2 and 3, and 960 time steps for Gear 4. All cases used 10 pseudo-time iterations per physical time step.

CFD runs were made for four gears and the disc at a number of rotation speeds. All cases were run for at least two complete revolutions to remove simulation startup transient behavior. Convergence histories show that transients leave the solution after about one revolution, as illustrated in Figure 11, where it is also observed that pseudo-time residual drop approximately two orders of magnitude in each physical time step when 10 pseudo-time steps are used per physical time step.

Comparisons between the power loss results of Diab et al., (Ref. 8) and the *NPHASE-PSU* analysis are presented in Figure 12 for all four gears. The CFD analysis for all four gears exhibited very good agreement with experiment. The disc case, however, did not share this same level of agreement, as illustrated in Figure 13, where *NPHASE-PSU* results are seen to under-predict the measured power loss. In order to elucidate the reasons for the deterioration in solution accuracy observed for the disc case, a number of observations and studies were made. First, it is observed that the measured (and computed) windage loss power levels for the disc are much smaller than the comparably sized spur gear (Gear 1, $D \approx 300\text{ mm}$). This arises due to the absence of any azimuthal pressure variation in the disc flow. Torque losses are due entirely to viscous effects, and these are clearly under-predicted. Indeed the absolute magnitudes of loss under-prediction between the disc and Gear 1 are comparable (e.g. $\approx 50\text{ W}$ @ 600s^{-1}), so presumably this under prediction of shear is present in all of the gear simulations; however, its relative magnitude is small.

To explore this further, the low-Reynolds number Menter

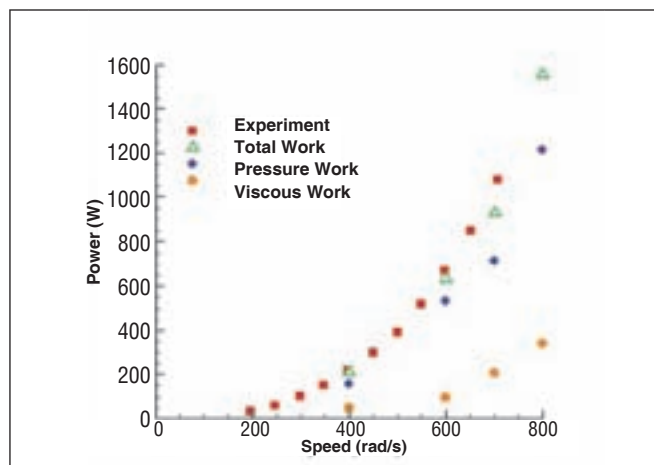


Figure 14—Breakdown of windage power losses for Diab 1.

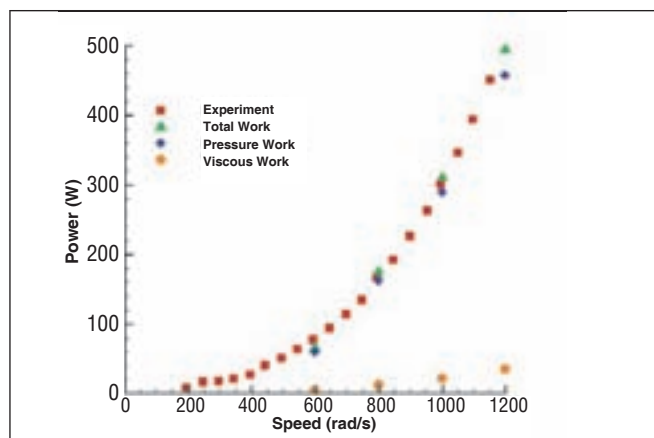


Figure 15—Breakdown of windage power losses for Diab 2.

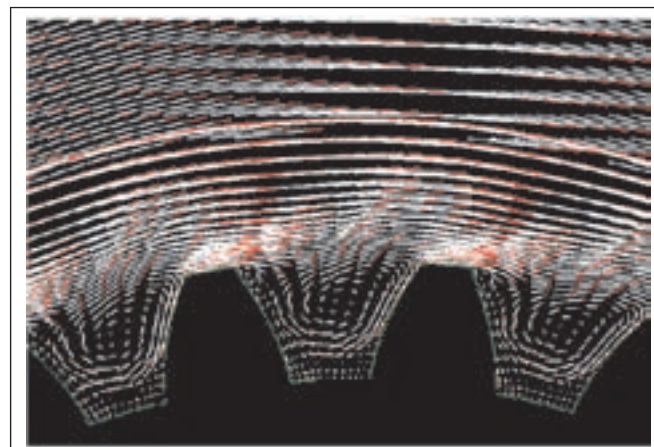


Figure 16—Predicted velocity vectors in the symmetry plane of a Diab gear.

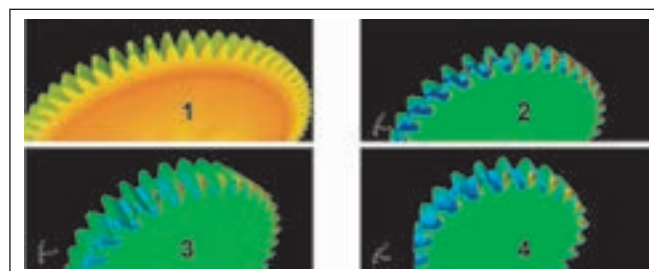


Figure 17—Predicted surface pressure distributions for the four Diab gears.

model was applied to the spinning disc case (using an appropriate sublayer resolved mesh). Figure 13 illustrates that improved turbulence modeling does benefit solution accuracy, especially at higher rotation rates. This observation is not as important for the gear cases since the spindown torques

associated with azimuthally varying pressure forces in the vicinity of the gear teeth dominate the viscous forces as shown in Figures 14 and 15. It can be seen that, especially at lower rotation rates, the contribution of viscous loss to total windage loss, is small. However, we do observe that at higher pitchline velocities, the relative magnitude of the viscous torque increases with respect to the pressure torque. This can be seen for higher rotation rates on Gear 1 (Fig. 14), as well as by considering the smaller size (and hence lower pitchline velocities) of Gear 2 (Fig. 5).

Results suggest that for the very high-speed gears to be encountered in rotorcraft (and other high-performance aircraft) transmissions, viscous effects will become more important than encountered here and will require attendant research attention.

Details of 3-D flow field. A number of important physical features of the predicted flow field are available upon interrogation of the CFD simulations. Figure 16 shows a view of the predicted secondary velocity vectors on the symmetry plane in the gear-relative frame of reference for one of the Diab cases. One can see a significant vortical structure within the gear tooth region, and the tooth-to-tooth periodicity that has been achieved in the transient simulation. Figure 17 shows a view of the predicted surface pressure distributions for the four Diab gears. There, comparatively large vs. small pressures are observed on the leading and trailing tooth faces, this difference being the source of the pressure component of the spin-down torque. The 3-D nature of the flow in these relatively low aspect ratio spurs gears is also clearly seen (figure shows only 1/2 of each gear). Significant 3-D effects are also clearly visualized in Figure 18, where gear-relative streamlines are displayed in the near-tooth region along with an isosurface of predicted static pressure in a region of high pressure.

Overset grid simulations. As of this writing, the overset capability for spinning gear simulations has been established in *NPHASE-PSU*. In this context, we are pursuing an overset verification effort and a relevant validation effort. The verification effort involves solving isolated spinning gear cases studied above using a rotating near-gear mesh and a stationary far-field mesh, the necessary approach to be used in ongoing gearbox windage activities. Figure 19 shows a view of an overset Diab Gear 4 simulation. Surface pressure contours are displayed, along with overset gear and background meshes on the symmetry plane. As expected, the CFD code returns nearly identical results for this moving grid overset simulation to the non-overset results reported above. We continue to parameterize gridding requirements in the overlap region, including the proximity of the overlap region to the gear in assessing the retained accuracy of the overset approach.

The validation effort under way involves simulating a series of shrouded low-speed gears for which windage loss measurements were made by Dawson (Ref. 7). To date, we have developed valid overset assembly grid topologies for

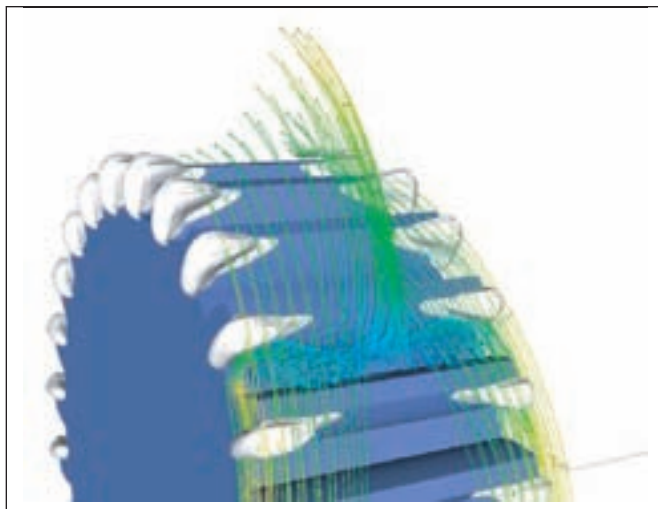


Figure 18—Predicted relative frame streamlines and isosurface of a high pressure region for Diab Gear 4.

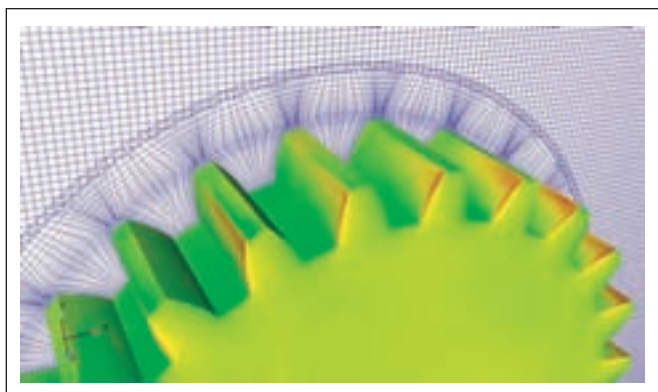


Figure 19—Verification study: 3-D overset grid solution and topology for Diab Gear 4.

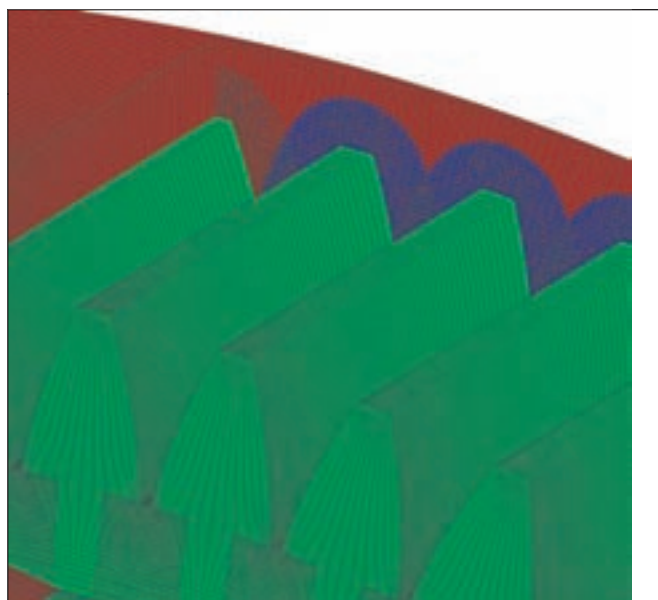


Figure 20—Validation study: 3-D overset grid topology for Dawson shrouded gear.

this, as shown in Figure 20, and anticipate reporting CFD analysis for these configurations in the near future.

Conclusion

This paper has summarized the adaptation and validation status of a CFD method for gear windage aerodynamics. Validation studies of 3-D spur gears in free space demonstrate very good agreement with published data. The following conclusions apply:

1) Viscous/turbulence modeling was identified as a shortcoming since loss power was consistently under-predicted for the viscous-drag-only spinning disc cases.

2) Low-Reynolds number (sublayer resolved) turbulence modeling exhibited improved performance for this case.

3) High-Reynolds number two equation modeling proved appropriate for modeling the moderate speed Diab spur gear suite, due apparently to the dominance of the pressure torques on spin-down.

4) The budgets of viscous and pressure components of spin-down torque suggest that viscous effects will become much more important, perhaps exceeding 50%, for gears with pitchline speeds approaching twice that investigated here.

5) Overset meshing is and will continue to be a critical enabler in this effort. The capability has been established and demonstrated here and will become integral in further studies where the isolated gear assumption will not be relevant. 

Acknowledgments

This work was supported by NASA under NASA Cooperative agreement NNX07AB34A.

References

1. Winfree, D. "Reducing Gear Windage Losses from High-Speed Gears," ASME Power Transmission and Gearing Conference, ASME, Baltimore, MD, Sept., 2000.
2. Anderson, N. and S. Loewenthal, "Spur-Gear-System Efficiency at Part and Full Load," Tech. Rep., NASA, 10 Dec. 10, 1979, TP 1622 AVRADCOM TR 79-46.
3. Anderson, N. and S. Loewenthal, "Effect of Geometry and Operating Conditions of Spur Gear System Power Loss," *Journal of Mechanical Design*, Vol. 103, Jan., 1981, pp. 151-159.
4. Anderson, N. and S. Loewenthal, "Efficiency of Non-standard and High-Contact Ratio Involute Spur Gears," Fourth International Power Transmission and Gearing Conference, ASME, Cambridge, MA, Oct., 1984, NASA TM 83725 USAAVSCOM TR 84-C-9.
5. Handschuh, R. and C. Kilmain, "Preliminary Investigation of the Thermal Behavior of High-Speed Helical Gear Trains," International Conference on Gears, International Federation for the Theory of Machines and Mechanisms, Munich, Germany, March, 2002, NASA/TM-2002-211336 ARL-TR-2661.
6. Heingartner, P. and D. Mba, "Determining Power Losses in the Helical Gear Mesh," *Gear Technology*, Sept., 2005.
7. Dawson, P., "Windage Loss in Larger High-Speed Gears," *Proceedings Instn. Mech. Engrs.*, Vol. 198A, No. 1, 1984, pp. 51-59.
8. Diab, Y., F. Ville, P. Vexel and C. Changent, "Windage Losses in High-Speed Gears—Preliminary Experimental and Theoretical Results," *Journal of Mechanical Design*, Vol. 126, Sept., 2004, pp. 903-908.
9. Al-Shibli, K., K. Simmons and C. N. Eastwick, "Modelling Windage Power Loss from an Enclosed Spur Gear," *Journal of Power and Energy*, Vol. 221, 2007, pp. 331-341, Proc. IMechE Part A.
10. Eastwick, C. and G. Johnson, "Gear Windage: A Review," *Journal of Mechanical Energy*, Vol. 130, March, 2008.
11. Menter, F., "Two-Equation Eddy-Viscosity Turbulence Models for

Engineering Applications," *AIAA Journal*, Vol. 32, 1994, pp. 269-28912. Kunz, R., W. Yu, S. Antal and S. Eitorre, "An Unstructured Two-Fluid Model Based on the Coupled Phasic Exchange Algorithm," 15th AIAA Computational Fluid Dynamics Conference, Norfolk, VA, June, 2001, AIAA 2001-2672.

13. Clift, S. and P. Forsyth, "Linear and Non-Linear Methods for the Incompressible Navier-Stokes Equations," *International Journal for Numerical Methods in Fluids*, Vol. 18, 1994, pp. 229-256.

14. Van Doormal, J. and G. Raithby, "Enhancements of the SIMPLE Method for Predicting Incompressible Flows," *Numerical Heat Transfer*, Vol. 7, 1984, pp. 147-163.

15. Rhie, C. and W. Chow, "Numerical Study of the Turbulent Flow Past an Airfoil with Trailing Edge Separation," *AIAA Journal*, Vol. 21, 1983, pp. 1527.

16. Thomas, P. and C. Lombard, "Geometric Conservation Law and its Application to Flow Computations on Moving Grids," *AIAA Journal*, Vol. 17, 1979, pp. 1030-1037.

17. PETSC, <http://acts.nersc.gov/petsc>.

18. METIS, <http://glaros.dtc.umn.edu/gkhome/views/metis>.

19. Benek, J., J. Steger and F. Dougherty, "A Flexible Grid Embedding Technique with Applications to the Euler Equations," 1983, AIAA 83-1944.

20. Noack, R., "DiRTlib: A Library to Add an Overset Capability to Your Flow Solver," 17th AIAA Computational Fluid Dynamics Conference, AIAA, Toronto, Ontario, Canada, June, 2006, AIAA 2005-5116.

21. Noack, R., "SUGGAR: A General Capability for Moving Body Overset Grid Assembly," 17th AIAA Computational Fluid Dynamics Conference, AIAA, Toronto, Ontario, Canada, June, 2005, AIAA 2005-5117.

22. Schlichting, H., *Boundary Layer Theory*, McGraw-Hill, New York, 6th Ed., 1968.

23. *Pointwise*, Gridgen User Manual, Version 15.10, Ed., 2007.

Dr. Robert Handschuh

has more than 25 years of experience with NASA and the DOD in rotorcraft drive system analysis and experimental methods. Dr. Handschuh is currently leading research in high-speed gearing including performance and loss-of-lubrication technology.

Matthew Hill

is a doctoral candidate in aerospace engineering at The Pennsylvania State University. His principal research interests are computational fluid dynamics, grid generation, software engineering and rotorcraft aerodynamics.

Dr. Robert Kunz

is a senior research associate at The Penn State Applied Research Laboratory. He is an assistant director of ARL, heading the Computational Mechanics Division. Dr. Kunz is also on the graduate faculty of the university as an associate professor of aerospace engineering.

Dr. Lyle Long

is a distinguished professor of aerospace engineering, bioengineering, and mathematics at The Pennsylvania State University. He is the founder and director of the Graduate Minor Program in Computational Science (www.csci.psu.edu). He was also the founding editor-in-chief of the Journal of Aerospace Computing, Information and Communication.

Philip Morris

is the Boeing/A.D. Welliver professor of aerospace engineering at The Pennsylvania State University. He has served as the Drive Systems Team leader for the Mechanical Components Branch at NASA Glenn Research Center for over 10 years.

Dr. Ralph Noack

is a senior research associate at The Penn State Applied Research Laboratory. His principal research interests and activities include computational fluid dynamics, moving body simulations and overset grid technology.